Hindawi
Advances in High Energy Physics
Volume 2022, Article ID 5780441, 17 pages
https://doi.org/10.1155/2022/5780441

Research Article

Effects of Variations of SUSY Breaking Scale on Neutrino Parameters at Low Energy Scale under Radiative Corrections

Kh. Helensana Devi[1], **K. Sashikanta Singh**[1] and **N. Nimai Singh**[1,2]

[1]*Department of Physics, Manipur University, Imphal 795003, India*
[2]*Research Institute of Science and Technology, Imphal 795003, India*

Correspondence should be addressed to Kh. Helensana Devi; helensanakhumanthem2@manipuruniv.ac.in

Received 1 June 2022; Revised 21 August 2022; Accepted 6 October 2022; Published 16 November 2022

Academic Editor: Mariana Frank

The paper addresses the effects of the variations of the SUSY breaking scale m_s in the range (2-14) TeV on the three neutrino masses and mixings, in running the renormalization group equations (RGEs) for different input values of high energy seesaw scale M_R, and in both normal and inverted hierarchical neutrino mass models. The present investigation is a continuation of the earlier works based on the variation of m_s scale. Two approaches are adopted one after another—bottom-up approach for running gauge and Yukawa couplings from low to high energy scale, followed by the top-down approach from high to low energy scale for running neutrino parameters defined at high energy scale, along with gauge and Yukawa couplings. A self-complementarity relation among three mixing angles is also employed in the analysis and it is found to be stable under radiative correction. Significant effect due to radiative corrections on neutrino parameters with the variation of SUSY breaking scale m_s is observed. For comparison of the results, variation of tan β for different M_R is also considered.

1. Introduction

Neutrino physics has registered significant progress in recent years with the measurements of nonzero θ_{13} [1–3] and the Dirac CP phase [4, 5], thus indicating a possibility for a sizable CP violation in neutrino sector. The T2K team [5] has concluded with 3σ confidence level that the Dirac Phase δ_{CP} lies somewhere between -3.41 and -0.03 for normal hierarchy (NH) and between -2.54 and -0.32 for inverted hierarchy (IH). The interval includes the CP-conserving value of $-\pi = -22/7 = -3.14$ in case of NH, so that the CP conservation is disfavored only at the modest 2σ confidence level. Next generation of neutrino detectors, such as Hyper-Kamiokande in Japan, DUNE in USA, and JUNO in China, may be able to get 5σ confidence level for confirmation of CP violation in neutrino sector. Neutrino oscillations [6–8] have been well studied with the precise measurements of neutrino oscillation mass parameters and mixing angles. But till date, there are still some unsettled questions in neutrino physics such as the correct mass hierarchical order whether normal or inverted, absolute neutrino mass scale, nature of neutrinos whether Dirac or Majorana type, the exact high energy scale of seesaw mechanism, and the supersymmetric breaking scale if all it exists, to mention a few. The information related to the absolute neutrino masses has been continuously updating with the recent Planck data on cosmological upper bound [9, 10] on the sum of three absolute neutrino masses $\Sigma|m_i| < 0.12$ eV, neutrinoless double beta decay [11, 12] results with the upper limit on the effective Majorana neutrino mass $\langle m_{\beta\beta}\rangle < (0.036 - 0.156)$ eV from the KamLAND-Zen experiment [13] in Japan, and KATRIN [14] result on direct kinematic measurement with the upper bound $m_{\nu_e} < 0.8$ eV. Neutrino mass model, if any, is bound to be consistent with these upper bounds on absolute neutrino masses. On theoretical front, the presence of supersymmetry (SUSY) [15–17] enables us to ensure the stability of hierarchy between the weak and GUT scales with the possible cancellation of quadratic term in radiative corrections to the Higgs boson mass. It is needed to have a precise unification point of three gauge couplings at high

Table 1: Latest experimental data for fermion masses, gauge coupling constants, and Weinberg mixing angle.

Mass (GeV)	Coupling constants	Weinberg mixing angle
$m_Z(m_Z) = 91.1876$	$\alpha_{em}^{-1}(m_Z) = 127.952 \pm 0.009$	$\sin^2\theta_W(m_Z) = 0.23121 \pm 0.00017$
$m_t(m_t) = 172.76$	$\alpha_s(m_Z) = 0.1179 \pm 0.009$	
$m_b(m_b) = 4.18$		
$m_\tau(m_\tau) = 1.77$		

GUT scale around 2×10^{16} GeV [18–20]. It can also provide a natural mechanism for understanding the electroweak symmetry breaking (EWSB) [21, 22] and Higgs physics. Minimal Supersymmetric Standard Model (MSSM) [23] is thus a straightforward extension of the Standard Model (SM) with minimum number of new parameters. All the particles in the same supersymmetric multiplet would have the same mass if the supersymmetry is an exact symmetry. So far, there is no clear evidence for the presence of supersymmetric particles in the ongoing Large Hadron Collider (LHC), and LHC has almost reached its maximum energy of about 14 TeV [24, 25]. Third run of LHC reaches 13.6 TeV slightly higher than that of 13 TeV of the second run [26]. While the existence of supersymmetric particles has been continuously ruling out in LHC, the supersymmetric breaking scale (m_s) still remains as an unknown parameter. There are speculations that SUSY particles may have a wide spectrum and are not confined to a single energy scale. For simplicity, one can assume a single scale [27, 28] for all supersymmetric particles and this kind of assumption is valid as long as the m_Z or $m_t < < m_s$ [29, 30]. We assume that the m_s scale may lie somewhere in between 2 TeV and 14 TeV within the scope of LHC. The effects of the variations of SUSY breaking scale on the unification of gauge couplings and also Yukawa couplings in MSSM and SUSY GUT models have already been addressed using the two-loop RGEs for gauge and Yukawa couplings within the minimal supersymmetric SU(5) model [18], while ignoring for simplicity the threshold effects of the heavy particles, which could be as large as a few percentages. It has already been reported that for gauge couplings, the unification point increases with the increase in the SUSY breaking scale, but for Yukawa couplings the unification points decrease with the increase in SUSY breaking in the reverse order compared to the gauge couplings [18]. This finding has certain implications in other important issues such as running of the renormalization group equations (RGEs) [31–33] for neutrino masses and mixings from high energy seesaw scale to low energy electroweak scale. In this direction, a preliminary analysis with normal hierarchical model has already been carried out on the stability of neutrino parameters and self-complementarity relation [34] with varying SUSY breaking scale m_s.

The present investigation is a continuation of our previous work on neutrino masses and mixings with varying SUSY breaking scale in the running of RGEs [18, 22, 32, 35–38]. We shall address both normal hierarchical and inverted hierarchical neutrino mass models in both approaches—in the first place, the bottom-up approach for running gauge and Yukawa couplings from low to high energy scale; and in the second place, the top-down approach for running neutrino parameters defined at high energy scale, along with gauge and Yukawa couplings, from high to low energy scale. The present work is confined to the question of stability of neutrino mass models for both normal and inverted hierarchy with the variation of m_s scale and other input parameters $\tan\beta$ and M_R scale. Another important applications of RGE analysis such as low energy magnification of neutrino mixings in quark-lepton unification hypothesis at high energy scale, radiative correction to validate the tribimaximal mixings and golden ratio mixing at high scale, and radiative origin of reactor angle and solar neutrino mass-squared parameter at low energy scale are not addressed in the present investigations.

The paper is organised as follows. In Section 2, we give a brief discussion of gauge and Yukawa coupling RGEs mainly on bottom-up and top-down runnings. In Section 3, we present the numerical analysis and results. In Section 4, we study the effects of variations on neutrino parameters for different values of $\tan\beta$. Summary and Discussion are presented in Section 5. We give relevant RGEs for gauge, Yukawa, and quartic Higgs couplings in two-loops for both the SM and MSSM in Appendix A and RGEs of neutrino parameters in Appendix B.

2. Renormalization Group Equations (RGEs)

We study the radiative corrections to neutrino oscillation parameters using the Renormalisation Group Equations (RGEs) [18, 31, 39] with and without SUSY in two different steps using the low energy observational input values, bottom-up running from low to high energy scale for gauge and Yukawa couplings, and top-down running from high to low energy scale for neutrino mass parameters and mixing angles, along with gauge and Yukawa couplings which are already evaluated at high energy scale M_R.

2.1. Bottom-Up Running. In the bottom-up running of the RGEs, we divide it into three regions, $m_Z < \mu < m_t$, $m_t < \mu < m_s$, and $m_s < \mu < M_R$. We use the recent experimental data [8, 40] as initial input values at low energy scale, given in Table 1.

The values of gauge couplings, α_2 for $SU(2)_L$ and α_1 for $U(1)_Y$, are calculated by using $\sin^2\theta_W(m_Z) = \alpha_{em}(m_Z)/\alpha_2(m_Z)$ and matching condition,

$$\frac{1}{\alpha_{em}(m_Z)} = \frac{5}{3}\frac{1}{\alpha_1(m_Z)} + \frac{1}{\alpha_2(m_Z)}. \qquad (1)$$

We can also express the gauge couplings α_i's [18] in terms of normalized couplings g_i's as $g_i = \sqrt{4\pi\alpha_i}$, where $i = 1, 2, 3$ denote electromagnetic, weak, and strong couplings, respectively. RGEs at one-loop level [41] is used for evolution of the three gauge coupling constants from m_Z scale to m_t scale, as given below

$$\frac{1}{\alpha_i(\mu)} = \frac{1}{\alpha_i(m_Z)} - \frac{b_i}{2\pi} \ln \frac{\mu}{m_Z}, \tag{2}$$

where $m_Z \leq \mu \leq m_t$ and $b_i = (5.30, -0.50, -4.00)$ for non-SUSY case. For fermion masses to define at m_t scale, we use QED-QCD rescaling factor η [42], $m_b(m_t) = m_b(m_b)/\eta_b$, and $m_\tau(m_t) = m_\tau(m_\tau)/\eta_\tau$, where $\eta_b = 1.53$ and $\eta_\tau = 1.015$. We then convert them to Yukawa couplings, $h_t(m_t) = m_t(m_t)/v_0$, $h_b(m_t) = m_b(m_b)/v_0\eta_b$, and $h_\tau(m_\tau) = m_\tau(m_\tau)/v_0\eta_\tau$, where $v_0 = 174\,\text{GeV}$ is the vacuum expectation value (VEV) of SM Higgs field. The calculated numerical values for fermion masses, Yukawa, and gauge couplings at m_t scale are given in Table 2.

We study the effect of variation of SUSY breaking scale (m_s) on gauge and Yukawa couplings for running from m_t to the M_R scale using RGEs, which are given in Appendix A. At m_s scale, the following matching conditions are applied at the transition point from SM ($m_t < \mu < m_s$) to MSSM ($m_s < \mu < M_R$) as

$$\begin{aligned} g_i(\text{SUSY}) &= g_i(\text{SM}) \\ h_t(\text{SUSY}) &= \frac{h_t(\text{SM})}{\sin\beta} = h_t(\text{SM}) \times \frac{\sqrt{1+\tan^2\beta}}{\tan\beta}, \\ h_b(\text{SUSY}) &= \frac{h_b(\text{SM})}{\cos\beta} = h_b(\text{SM}) \times \sqrt{1+\tan^2\beta}, \\ h_\tau(\text{SUSY}) &= \frac{h_\tau(\text{SM})}{\cos\beta} = h_\tau(\text{SM}) \times \sqrt{1+\tan^2\beta}. \end{aligned} \tag{3}$$

Third generation Yukawa coupling constants are highly affected by input value of $\tan\beta$ as shown in Equation (3). A detailed numerical analysis shows that high scale value of h_t always decreases with input value on SUSY breaking scale m_s in the range (2-14) TeV for low and high $\tan\beta = 25, 35, 40, 45,$ and 55. However, high scale values of h_b and h_τ behave in different patterns. In fact h_b at high scale M_R increases with the increase of m_s scale for low value of $\tan\beta = 25$, but it decreases with m_s scale for higher values of $\tan\beta = 40 - 55$. For h_τ, it has a similar trend with h_b but with a little difference in the range of $\tan\beta$. In fact h_τ at high scale increases with the increase of m_s scale for both low and moderate values of $\tan\beta = 25, 40$, but it again decreases with m_s for higher value of $\tan\beta = 55$. For specific case used in the present calculation at input value of $\tan\beta = 40$, both h_t and h_b decrease with the increase of m_s scale, but h_τ increases with the increase of m_s scale. This analysis is reflected in Tables 3–6.

The output for Yukawa and gauge couplings at M_R scale are given in Table 3 for $M_R = 10^{13}$ GeV, Table 4 for $M_R = 10^{14}$ GeV, Table 5 for $M_R = 10^{15}$ GeV, and Table 6 for $M_R = 10^{16}$ GeV, respectively, for common value of $\tan\beta = 40$. These values are needed for the next top-down running as input values at high energy scale.

Table 2: Numerical values for fermion masses, Yukawa, and gauge couplings at m_t scale.

Fermions masses	Yukawa couplings	Gauge couplings
$m_t(m_t) = 172.76$ GeV	$h_t(m_t) = 0.9928$	$g_1(m_t) = 0.4635$
$m_b(m_t) = 2.73$ GeV	$h_b(m_t) = 0.0157$	$g_2(m_t) = 0.6511$
$m_\tau(m_t) = 1.75$ GeV	$h_\tau(m_t) = 0.0100$	$g_3(m_t) = 1.1890$

Table 3: Values of Yukawa and gauge couplings evaluated at $t_R = \ln(10^{13}\,\text{GeV}) = 29.93$ for $\tan\beta = 40$, for different choices of m_s scale.

m_s (TeV)	h_t	h_b	h_τ	g_1	g_2	g_3
2	0.6509	0.3139	0.3721	0.6086	0.6914	0.7743
4	0.6318	0.3102	0.3741	0.6043	0.6861	0.7700
6	0.6236	0.3086	0.3750	0.6023	0.6835	0.7679
8	0.6161	0.3071	0.3760	0.6002	0.6810	0.7658
10	0.6126	0.3063	0.3765	0.5992	0.6797	0.7648
12	0.6093	0.3056	0.3770	0.5981	0.6785	0.7638
14	0.6061	0.3050	0.3775	0.5971	0.6772	0.7628

Table 4: Values of Yukawa and gauge couplings evaluated at $t_R = \ln(10^{14}\,\text{GeV}) = 32.23$ for $\tan\beta = 40$, for different choices of m_s scale.

m_s(TeV)	h_t	h_b	h_τ	g_1	g_2	g_3
2	0.6289	0.2977	0.3650	0.6316	0.6982	0.7554
4	0.6104	0.2946	0.3674	0.6268	0.6915	0.7514
6	0.6022	0.2931	0.3684	0.6245	0.6889	0.7495
8	0.5947	0.2917	0.3695	0.6222	0.6863	0.7475
10	0.5913	0.2910	0.3700	0.6211	0.6850	0.7466
12	0.5879	0.2904	0.3705	0.6199	0.6837	0.7456
14	0.5848	0.2898	0.3710	0.6188	0.6824	0.7447

2.2. Top-Down Running. In this running, we use the values of Yukawa and guage couplings which are found at M_R scale as initial inputs given in Tables 3–6. In this work, the high energy seesaw scale is the starting point for running the RGEs and it ends at electroweak scale. We give the sum of three neutrino masses $\Sigma|m_i|$ in the range, 0.114 eV -0.121 eV for NH case and 0.1056 eV -0.1072 eV for IH case. The input values of neutrino masses and three mixing angles are indeed arbitrary in order to study the stability of neutrino mass model under RGEs running at low scale, with variations of other free parameters such as $\tan\beta$, SUSY breaking scale m_s, and high energy scale M_R. We select our input values in Tables 7–8 with the aim to produce low energy values of neutrino oscillation parameters consistent with observational data. In our work, we focus on the high energy seesaw scale at $M_R = 10^{14}$ GeV; but for comparison, it has been supplemented by other values of high energy

Table 5: Values of Yukawa and gauge couplings $t_R = \ln(10^{15}$ GeV$) = 34.53$ for $\tan\beta = 40$, for different choices of m_s scale.

m_s (TeV)	h_t	h_b	h_τ	g_1	g_2	g_3
2	0.6084	0.2829	0.3579	0.6574	0.7026	0.7378
4	0.5891	0.2798	0.3601	0.6521	0.6971	0.7341
6	0.5809	0.2784	0.3613	0.6494	0.6944	0.7323
8	0.5735	0.2771	0.3624	0.6468	0.6917	0.7305
10	0.5701	0.2766	0.3629	0.6455	0.6903	0.7296
12	0.5668	0.2760	0.3635	0.6443	0.6890	0.7287
14	0.5637	0.2754	0.3640	0.6430	0.6877	0.7278

Table 6: Values of Yukawa and gauge couplings evaluated at $t_R = \ln(10^{16}$ GeV$) = 36.84$ for $\tan\beta = 40$, for different choices of m_s scale.

m_s (TeV)	h_t	h_b	h_τ	g_1	g_2	g_3
2	0.5854	0.2676	0.3494	0.6893	0.7089	0.7200
4	0.5661	0.2647	0.3518	0.6831	0.7032	0.7166
6	0.5580	0.2634	0.3529	0.6801	0.7004	0.7149
8	0.5680	0.2687	0.3622	0.6770	0.6664	0.7131
10	0.5473	0.2618	0.3547	0.6757	0.6963	0.7124
12	0.5441	0.2613	0.3553	0.6742	0.6949	0.7116
14	0.5410	0.2608	0.3559	0.6727	0.6936	0.7107

Table 7: Input set of neutrino parameters at high energy scale M_R for NH case. θ_{23} is used from SC relation, $\theta_{23} = q \times (\theta_{13} + \theta_{12})$ with $q = 1.1$. This is common for all cases of m_s scale.

Input parameters	Seesaw scale ($\tan\beta = 40$)			
	10^{16} GeV	10^{15} GeV	10^{14} GeV	10^{13} GeV
m_1(eV)	0.0262	0.0258	0.0271	0.0274
m_2(eV)	-0.0263	-0.0259	-0.0272	-0.0275
m_3(eV)	-0.0615	-0.0645	-0.0643	-0.0664
$\Sigma\|m_i\|$	0.114	0.116	0.118	0.121
$\theta_{12}/^0$	32.46	33.95	33.01	32.61
$\theta_{13}/^0$	7.39	7.56	7.64	7.70
$\psi_1/^0 = \psi_2/^0 = \psi/^0$	180	180	180	180
$\delta_{CP}/^0$	240	240	240	240

scales ($M_R = 10^{13}$ GeV, 10^{15} GeV, and 10^{16} GeV). For input values of mixing angles, we impose a phenomenological relation of lepton mixing angles known as self-complementarity relation (SC), $\theta_{23} = q(\theta_{12} + \theta_{13})$ [43–50]. In this work, we take $q = 1.1$ for fine tuning and we study the stability of SC relation against RGEs. It is observed that this SC relation is nearly stable under radiative corrections. The SC relation for lepton mixing angles is phenomenologically analogous to a relation for quark and lepton mixing angles known as Quark-Lepton Complementarity (QLC) relations, $\theta_{sun} + \theta_C = \pi/4$ [43, 44, 46, 47] between the leptonic 1-2 mixing angle θ_{sun} and the Cabibbo angle θ_C. We also impose the following conditions on input values of neutrino masses.

Table 8: Input set of neutrino parameters at high energy scale M_R for IH case ($m_3 \neq 0$). θ_{23} is used from SC relation, $\theta_{23} = q \times (\theta_{13} + \theta_{12})$ with $q = 1.1$. This is common for all cases of m_s scale.

Input parameters	Seesaw scale ($\tan\beta = 40$)			
	10^{16} GeV	10^{15} GeV	10^{14} GeV	10^{13} GeV
m_1(eV)	0.0515	0.0501	0.0511	0.0523
m_2(eV)	-0.0516	-0.0502	-0.0512	-0.0524
m_3(eV)	-0.0025	-0.0021	-0.0022	-0.0025
$\Sigma\|m_i\|$	0.1056	0.1024	0.1045	0.1072
$\theta_{12}/^0$	31.94	32.39	31.99	32.17
$\theta_{13}/^0$	8.53	8.29	8.35	8.40
$\psi_1/^0 = \psi_2/^0 = \psi/^0$	180	180	180	180
$\delta_{CP}/^0$	240	240	240	240

The sum of the three neutrino masses should satisfy the latest Planck cosmological data $\Sigma|m_i| < 0.12$ eV,

(i) The neutrino mass model should be nearly quasidegenerate at least in m_1 and m_2 in order to get high value of θ_{13}, and m_3 should be nonzero

One can also express the neutrino mass eigenvalues after absorbing the Majorana CP phases as diag.$(m_1 e^{i\psi_1}, m_2 e^{i\psi_2}, m_3)$. As discussed in ref. [33], from the presence of a term $|m_1 e^{i\psi_1} + m_2 e^{i\psi_2}|/\Delta m^2_{21}$ in the evolution of θ_{12}, a nonzero value of the difference $|\psi_1 - \psi_2|$ of the Majorana phases damps the RG equation. The damping becomes maximal if this difference equals π, which corresponds to an opposite CP parity of the two nearly degenerate mass eigenstates m_1 and m_2. A similar term $|m_1 e^{i\psi_1} + m_3|/\Delta m^2_{31}$ is also present in the evolution equation of θ_{13}, and this implies opposite CP parity between m_1 and m_3, though they are not so degenerate. Under this consideration, we make our input choice of CP parity as diag.$(m_1, -m_2, -m_3)$ in the present work. The RGEs for evolution of θ_{12} is also directly proportional to a term $A_{21} = (m_2 + m_1)/(m_2 - m_1)$ which is highly sensitive for the nearly degenerate masses between m_1 and m_2 [22, 33]. Any possible singularity in the running of RGEs may be avoided with the choice of opposite CP parity between m_1 and m_2 for nearly degenerate case. In this work, we take two Majorana phases ψ_1 and ψ_2 at 180^0, which are constrained to be equal for simplicity ($\psi_1 = \psi_2 = \psi$), and the Dirac CP phase δ_{CP} angle at 240^0. Our main aim is to study the neutrino oscillation parameters against varying m_s for different M_R scale.

Using all the necessary mathematical frameworks, we analyze the radiative nature of neutrino parameters like neutrino masses, mixings, and CP phases in the top-down approach with the variations of m_s scale at different M_R scale. The respective RGEs which are given in Appendix B. The input sets are given in Tables 7 and 8.

3. Numerical Analysis and Results

The effects of the variation of m_s on the outputs of neutrino mass parameters and mixing angles are given in

Table 9: Effects on the output of neutrino parameters at low energy scale, on varying m_s for NH case ($\tan\beta = 40$, $M_R = 10^{13}$ GeV).

m_s scale (TeV)	$\Delta m^2_{31}\left(10^{-3}\,\mathrm{eV}^2\right)$	$\Delta m^2_{21}\left(10^{-5}\,\mathrm{eV}^2\right)$	$\theta_{23}\left(/^0\right)$	$\theta_{12}\left(/^0\right)$	$\theta_{13}\left(/^0\right)$	$\delta_{CP}\left(/^0\right)$	$\Sigma\lvert m_i\rvert$ (eV)
2	2.504	4.831	45.37	32.69	8.40	235.26	0.095
4	2.569	5.961	45.42	32.72	8.47	235.36	0.094
6	2.593	6.666	45.45	32.73	8.52	235.41	0.094
8	2.614	6.962	45.47	32.74	8.54	235.43	0.094
10	2.621	7.288	45.48	32.75	8.56	235.45	0.093
12	2.624	7.526	45.50	32.75	8.58	235.47	0.093
14	2.620	7.779	45.52	32.76	8.60	235.49	0.092

Table 10: Effects on the output of neutrino parameters at low energy scale, on varying m_s for NH case ($\tan\beta = 40$, $M_R = 10^{14}$ GeV).

m_s scale (TeV)	$\Delta m^2_{31}\left(10^{-3}\,\mathrm{eV}^2\right)$	$\Delta m^2_{21}\left(10^{-5}\,\mathrm{eV}^2\right)$	$\theta_{23}\left(/^0\right)$	$\theta_{12}\left(/^0\right)$	$\theta_{13}\left(/^0\right))$	$\delta_{CP}\left(/^0\right)$	$\Sigma\lvert m_i\rvert$ (eV)
2	2.336	4.771	45.75	32.09	8.35	235.08	0.092
4	2.418	5.850	45.79	32.11	8.41	235.16	0.093
6	2.428	6.541	45.82	33.13	8.46	235.22	0.092
8	2.435	6.859	45.84	33.14	8.48	235.24	0.091
10	2.440	7.180	45.86	33.15	8.51	235.27	0.091
12	2.441	7.490	45.88	33.16	8.53	235.29	0.090
14	2.454	7.654	45.89	33.16	8.55	235.30	0.090

Table 11: Effects on the output of neutrino parameters at low energy scale, on varying m_s for NH case ($\tan\beta = 40$, $M_R = 10^{15}$ GeV).

m_s scale (TeV)	$\Delta m^2_{31}\left(10^{-3}\,\mathrm{eV}^2\right)$	$\Delta m^2_{21}\left(10^{-5}\,\mathrm{eV}^2\right)$	$\theta_{23}\left(/^0\right)$	$\theta_{12}\left(/^0\right)$	$\theta_{13}\left(/^0\right)$	$\delta_{CP}\left(/^0\right)$	$\Sigma\lvert m_i\rvert$(eV)
2	2.373	4.371	46.71	34.03	8.24	235.35	0.090
4	2.461	5.350	46.76	34.05	8.31	235.43	0.090
6	2.479	5.964	46.79	34.07	8.35	235.48	0.090
8	2.492	6.264	46.81	34.08	8.38	235.51	0.090
10	2.498	6.633	46.83	34.09	8.41	235.54	0.089
12	2.498	6.832	46.84	34.09	8.43	235.56	0.089
14	2.499	7.028	46.86	34.10	8.45	235.57	0.088

Table 12: Effects on the output of neutrino parameters at low energy scale, on varying m_s for NH case ($\tan\beta = 40$, $M_R = 10^{16}$ GeV).

m_s scale (TeV)	$\Delta m^2_{31}\left(10^{-3}\,\mathrm{eV}^2\right)$	$\Delta m^2_{21}\left(10^{-5}\,\mathrm{eV}^2\right)$	$\theta_{23}\left(/^0\right)$	$\theta_{12}\left(/^0\right)$	$\theta_{13}\left(/^0\right)$	$\delta_{CP}\left(/^0\right)$	$\Sigma\lvert m_i\rvert$ (eV)
2	2.354	4.435	44.83	32.54	8.08	234.98	0.093
4	2.427	5.459	44.87	32.56	8.14	235.07	0.094
6	2.444	6.108	44.89	32.57	8.18	235.13	0.094
8	2.472	6.457	44.91	32.58	8.20	235.16	0.094
10	2.476	6.734	44.92	32.59	8.22	235.18	0.093
12	2.475	7.033	44.94	32.60	8.24	235.21	0.093
14	2.486	7.182	44.95	32.60	8.26	235.22	0.093

Tables 9–12, along with the graphical representations in Figure 1 for normal hierarchical (NH) model, and in Tables 13–16 and Figure 2 for inverted hierarchical (IH) case. In each case, we also present the results for variation of high energy seesaw scale (10^{13} -10^{16}) GeV. Similar patterns with the variations of seesaw scale are observed in all the Figures 1 and 2.

The neutrino oscillation parameters are found to be almost stable with the variation of m_s at low energy scale except Δm^2_{21} which is found to be very sensitive with the

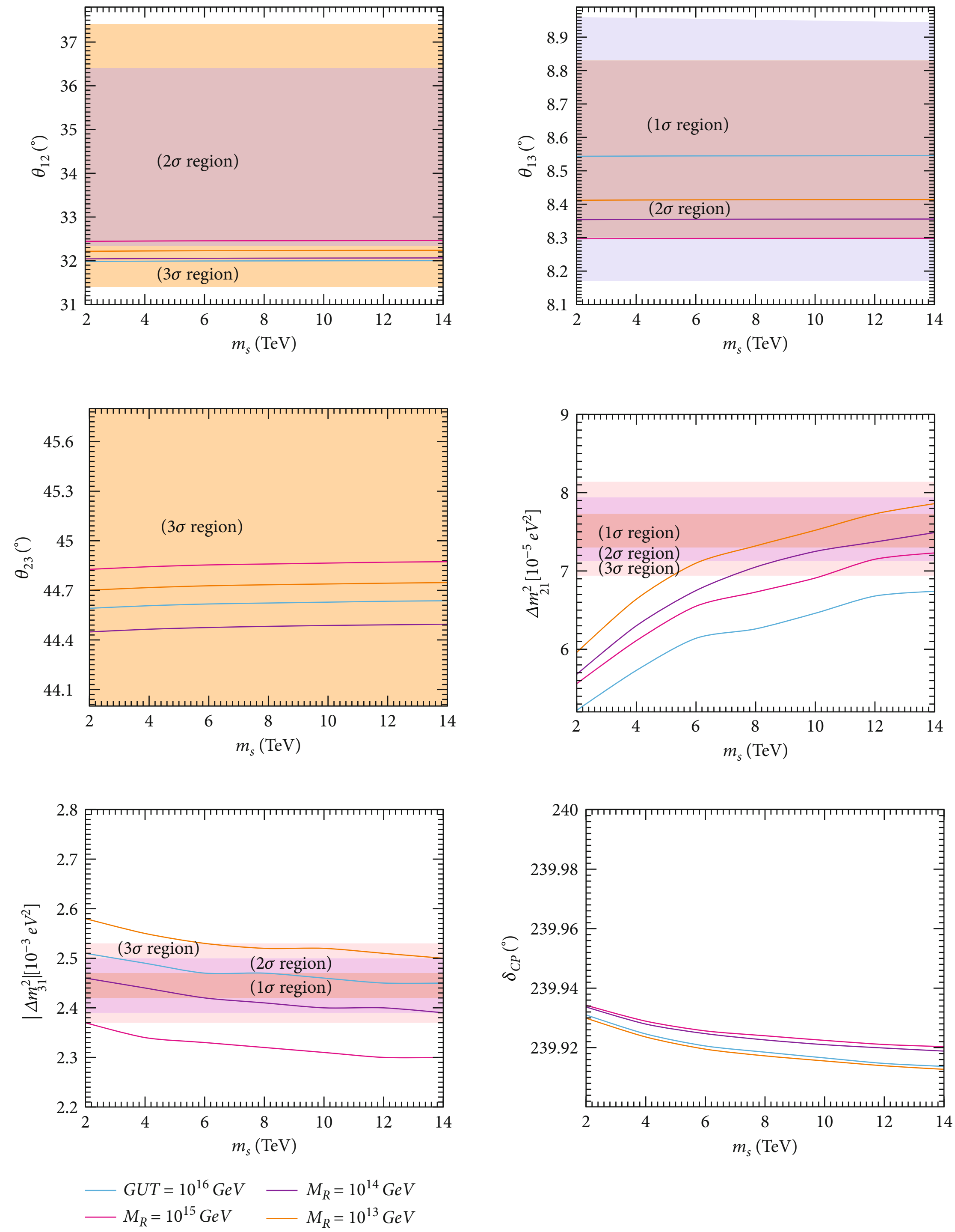

FIGURE 1: Effects on the low energy output results in θ_{ij}, $|\Delta m^2_{ij}|$, and δ_{CP} with variation of m_s for IH case at $\tan\beta = 40$. Four different choices of M_R scale are presented.

change of m_s scale. One difference between NH and IH model is that in NH case, all the low energy parameters Δm^2_{31}, Δm^2_{21}, θ_{23}, θ_{12}, θ_{13}, and δ_{CP} are found to increase with the increase of m_s scale, but in IH case, Δm^2_{21}, θ_{23}, and θ_{12} increase whereas $|\Delta m^2_{31}|$ and δ_{CP} decrease with m_s. The low energy values of $\Sigma|m_i|$ are below the latest Planck data $\Sigma|m_i| < 0.12$ eV, where the values for NH are smaller than those of IH case.

4. Effects of the Simultaneous Variation of m_s and $\tan\beta$ Values

In this section, we again study how the estimated low energy values of neutrino oscillation parameters behave with the simultaneous variations of m_s and $\tan\beta$ over a wide range. As a representative case, we consider only one seesaw scale

Table 13: Effects on the output of neutrino parameters at low energy scale, on varying m_s for IH case ($\tan\beta = 40$, $M_R = 10^{13}$ GeV).

m_s scale (TeV)	$\lvert\Delta m^2_{31}\rvert\,(10^{-3}\,\mathrm{eV}^2)$	$\Delta m^2_{21}\,(10^{-5}\,\mathrm{eV}^2)$	$\theta_{23}\,(/^0)$	$\theta_{12}\,(/^0)$	$\theta_{13}\,(/^0)$	$\delta_{CP}\,(/^0)$	$\Sigma\lvert m_i\rvert$(eV)
2	2.58	5.96	44.70	32.21	8.41	239.94	0.119
4	2.55	6.64	44.71	32.22	8.41	239.93	0.117
6	2.53	7.10	44.72	32.22	8.41	239.93	0.116
8	2.52	7.32	44.73	32.23	8.41	239.92	0.115
10	2.52	7.52	44.73	32.23	8.41	239.92	0.114
12	2.51	7.73	44.74	32.23	8.41	239.92	0.114
14	2.50	7.86	44.74	32.23	8.41	239.92	0.113

Table 14: Effects on the output of neutrino parameters at low energy scale, on varying m_s for IH case ($\tan\beta = 40$, $M_R = 10^{14}$ GeV).

m_s scale (TeV)	$\lvert\Delta m^2_{31}\rvert\,(10^{-3}\,\mathrm{eV}^2)$	$\Delta m^2_{21}\,(10^{-5}\,\mathrm{eV}^2)$	$\theta_{23}\,(/^0)$	$\theta_{12}\,(/^0)$	$\theta_{13}\,(/^0)$	$\delta_{CP}\,(/^0)$	$\Sigma\lvert m_i\rvert$(eV)
2	2.46	5.68	44.44	32.04	8.35	239.95	0.114
4	2.44	6.30	44.46	32.05	8.35	239.94	0.112
6	2.42	6.75	44.47	32.05	8.35	239.93	0.110
8	2.41	7.05	44.48	32.05	8.35	239.93	0.106
10	2.40	7.25	44.48	32.06	8.35	239.93	0.109
12	2.40	7.37	44.49	32.06	8.35	239.93	0.108
14	2.39	7.49	44.49	32.06	8.35	239.92	0.108

Table 15: Effects on the output of neutrino parameters at low energy scale, on varying m_s for IH case ($\tan\beta = 40$, $M_R = 10^{15}$ GeV).

m_s scale (TeV)	$\lvert\Delta m^2_{31}\rvert\,(10^{-3}\,\mathrm{eV}^2)$	$\Delta m^2_{21}\,(10^{-5}\,\mathrm{eV}^2)$	$\theta_{23}\,(/^0)$	$\theta_{12}\,(/^0)$	$\theta_{13}\,(/^0)$	$\delta_{CP}\,(/^0)$	$\Sigma\lvert m_i\rvert$(eV)
2	2.37	5.56	44.82	32.44	8.29	239.95	0.111
4	2.34	6.11	44.84	32.45	8.29	239.94	0.109
6	2.33	6.55	44.85	32.45	8.29	239.94	0.107
8	2.32	6.73	44.85	32.45	8.29	239.93	0.107
10	2.31	6.91	44.86	32.46	8.29	239.93	0.106
12	2.30	7.15	44.87	32.46	8.29	239.93	0.105
14	2.30	7.23	44.87	32.46	8.29	239.93	0.105

Table 16: Effects on the output of neutrino parameters at low energy scale, on varying m_s for IH case ($\tan\beta = 40$, $M_R = 10^{16}$ GeV). Four different choices of M_R scale are presented.

m_s scale (TeV)	$\lvert\Delta m^2_{31}\rvert\,(10^{-3}\,\mathrm{eV}^2)$	$\Delta m^2_{21}\,(10^{-5}\,\mathrm{eV}^2)$	$\theta_{23}\,(/^0)$	$\theta_{12}\,(/^0)$	$\theta_{13}\,(/^0)$	$\delta_{CP}\,(/^0)$	$\Sigma\lvert m_i\rvert$ (eV)
2	2.51	5.22	44.59	31.98	8.54	239.94	0.118
4	2.49	5.73	44.60	31.98	8.54	239.93	0.116
6	2.47	6.14	44.61	31.99	8.54	239.93	0.115
8	2.47	6.26	44.62	31.99	8.54	239.92	0.114
10	2.46	6.46	44.62	31.99	8.54	239.92	0.114
12	2.45	6.68	44.63	32.00	8.54	239.92	0.113
14	2.45	6.74	44.63	32.00	8.54	239.92	0.112

at $M_R = 10^{14}$ GeV for both NH and IH, using the same high scale input parameters given in Tables 7 and 8, respectively. We consider the range of $\tan\beta = 25 - 55$ along with the range of $m_s = (2 - 14)$ TeV. Significant effects of the variation of $\tan\beta$ for a given m_s value have been observed as shown in Tables 17 and 18 and Figures 3 and 4. The following observations on the low energy neutrino oscillation parameters can be drawn.

(i) All the three mixing angles are observed to increase with increasing values of $\tan\beta$ and m_s for both NH and IH cases

For NH case, both Δm^2_{21} and $\lvert\Delta m^2_{31}\rvert$ decrease with increasing value of $\tan\beta$, but increase with increasing m_s. For IH case, Δm^2_{21} increases but $\lvert\Delta m^2_{31}\rvert$ decreases with the increase of both $\tan\beta$ and m_s.

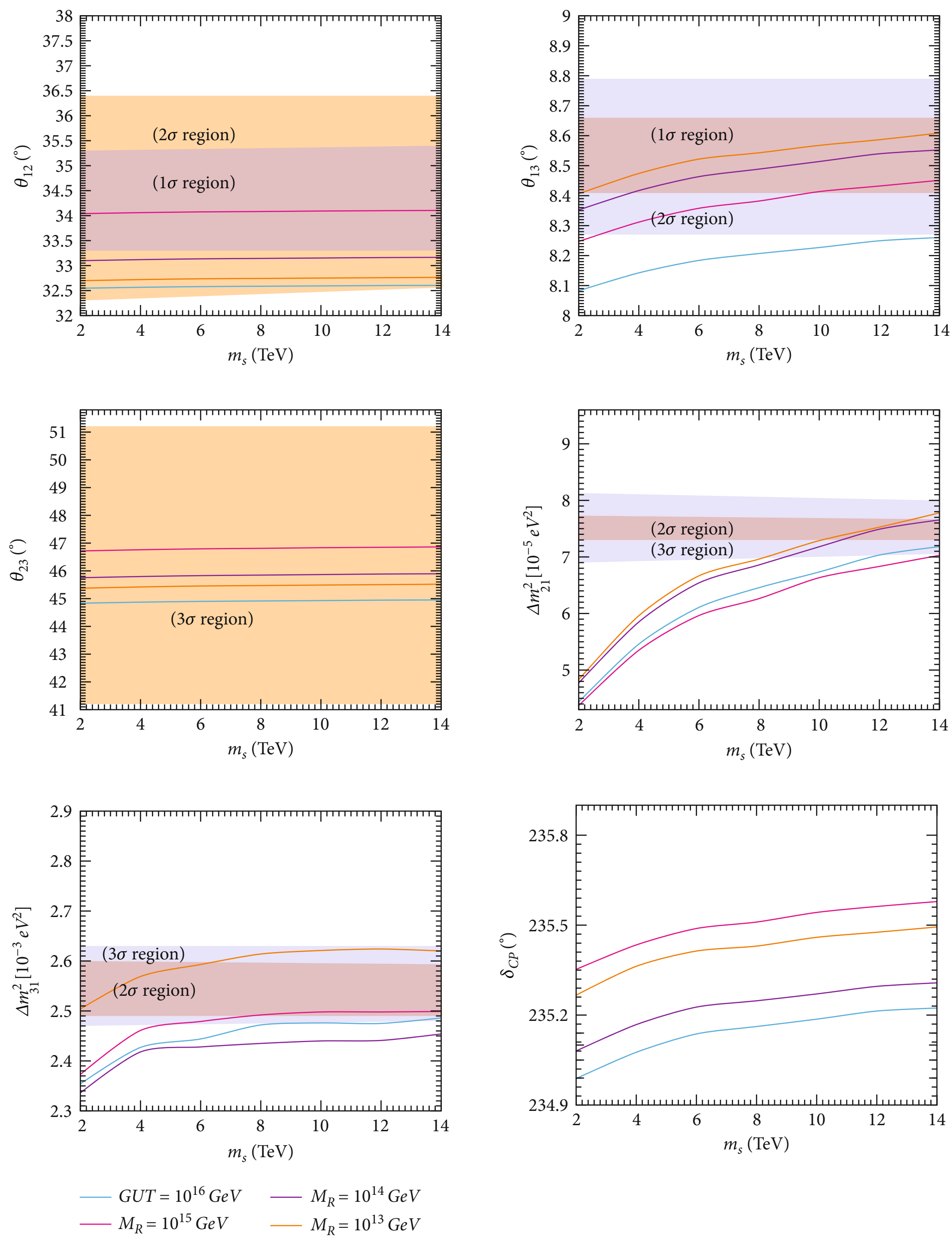

FIGURE 2: Effects on the low energy output results in θ_{ij}, $|\Delta m^2_{ij}|$, and δ_{CP} with variation of m_s for NH case at tan $\beta = 40$. Four different choices of M_R scale are presented.

For NH case, δ_{CP} decreases with increasing tan β but increases with increasing m_s, whereas for IH case, δ_{CP} decreases with the increase of both tan β and m_s.

5. Summary and Discussion

To summarize, the present work is a continuation of the earlier investigations [18, 32] on the effect of the variations of SUSY breaking scale m_s in the running of RGEs for neutrino masses and mixing parameters from high to low energy scale. Among many other applications of RGEs on neutrino physics such as magnification of neutrino mixings at low energy scale in quark-lepton unification hypothesis at high energy scale, generation of suitable radiative corrections to validate the tribimaximal or golden ratio neutrino mixings at high scale, and radiative origin of reactor mixing angle

Table 17: Effects on the neutrino oscillation parameters at low energy scale, on varying m_s and $\tan\beta$ for NH case ($M_R = 10^{14}$ GeV).

m_s (TeV)		$\tan\beta = 55$	$\tan\beta = 45$	$\tan\beta = 40$	$\tan\beta = 35$	$\tan\beta = 25$
2		46.63	45.85	45.75	44.25	43.96
4		46.64	45.88	45.79	44.29	44.00
6		46.64	45.91	45.82	44.31	44.02
8	$\theta_{23}/^0$	46.64	45.92	45.84	44.32	44.04
10		46.65	45.93	45.86	44.35	44.06
12		46.65	45.94	45.88	44.36	44.07
14		46.66	45.95	45.89	44.36	44.07
2		32.95	32.79	32.09	31.82	31.38
4		33.21	33.17	32.82	32.21	32.01
6		33.23	33.19	33.13	32.43	32.14
8	$\theta_{12}/^0$	33.28	33.21	33.14	32.54	32.18
10		33.29	33.23	33.15	32.63	32.28
12		33.31	33.26	33.16	32.66	32.29
14		33.33	33.28	33.16	32.67	32.31
2		8.96	8.42	8.35	8.14	7.95
4		9.02	8.48	8.41	8.20	8.00
6		9.04	8.53	8.46	8.23	8.02
8	$\theta_{13}/^0$	9.06	8.54	8.48	8.25	8.04
10		9.09	8.57	8.51	8.28	8.06
12		9.11	8.59	8.53	8.30	8.07
14		9.12	8.61	8.55	8.30	8.08
2		4.18	4.36	4.77	4.80	4.83
4		5.23	5.36	5.85	5.96	6.02
6		5.56	5.76	6.54	6.61	6.74
8	$\Delta m^2_{21}\left(10^{-5}\ \mathrm{eV}^2\right)$	6.08	6.21	6.85	6.91	7.01
10		6.37	6.59	7.18	7.23	7.38
12		6.76	6.82	7.49	7.51	7.69
14		6.88	7.11	7.65	7.71	7.89
2		2.04	2.32	2.33	2.45	2.56
4		2.09	2.36	2.41	2.49	2.60
6		2.14	2.39	2.42	2.52	2.63
8	$\left\|\Delta m^2_{31}\right\|\left(10^{-3}\ \mathrm{eV}^2\right)$	2.16	2.40	2.43	2.54	2.64
10		2.16	2.41	2.44	2.55	2.65
12		2.17	2.41	2.44	2.56	2.66
14		2.18	2.42	2.45	2.57	2.67
2		230.15	234.35	235.08	236.72	238.39
4		230.49	234.49	235.16	236.81	238.43
6		230.49	234.58	235.22	236.84	238.45
8	$\delta_{CP}/^0$	230.68	234.62	235.24	236.86	238.46
10		230.77	234.66	235.27	236.90	238.48
12		230.90	234.70	235.29	236.92	238.49
14		231.00	234.73	235.30	236.92	238.50

and solar neutrino mass-squared parameter at low energy; the present work focuses only on the question of the stability of neutrino mass models for both NH and IH, under RGEs analysis with the variations of SUSY breaking scale m_s and input value of $\tan\beta$.

The numerical analysis in the present investigation is confined to the effects on the variations of three important free parameters in the ranges—high energy seesaw scale $M_R = (10^{13} - 10^{16})$ GeV, the SUSY breaking scale $m_s = (2 - 14)$ TeV, and $\tan\beta = (25 - 55)$. As a special

Table 18: Effects on the neutrino oscillation parameters at low energy scale, on varying m_s and $\tan\beta$ for IH case ($M_R = 10^{14}$ GeV).

m_s(TeV)		$\tan\beta = 55$	$\tan\beta = 45$	$\tan\beta = 40$	$\tan\beta = 35$	$\tan\beta = 25$
2		44.58	44.46	44.44	44.41	44.38
4		44.62	44.49	44.46	44.42	44.39
6		44.64	44.50	44.47	44.43	44.39
8	$\theta_{23}/^0$	44.66	44.51	44.48	44.44	44.40
10		44.67	44.52	44.48	44.44	44.40
12		44.68	44.52	44.49	44.44	44.40
14		44.69	44.53	44.49	44.45	44.40
2		32.078	32.058	32.048	32.026	32.001
4		32.083	32.061	32.051	32.029	32.008
6		32.088	32.068	32.052	32.031	32.016
8	$\theta_{12}/^0$	32.096	32.071	32.056	32.036	32.021
10		32.101	32.076	32.061	32.042	32.026
12		32.108	32.081	32.064	32.044	32.031
14		32.111	32.083	32.067	32.046	32.033
2		8.378	8.362	8.351	8.339	8.329
4		8.379	8.363	8.351	8.342	8.332
6		8.381	8.364	8.352	8.345	8.334
8	$\theta_{13}/^0$	8.383	8.366	8.353	8.347	8.336
10		8.385	8.369	8.354	8.348	8.338
12		8.388	8.371	8.355	8.351	8.339
14		8.390	8.372	8.356	8.353	8.340
2		12.48	7.98	5.68	5.55	4.38
4		13.95	9.08	6.30	6.08	4.93
6		14.42	9.43	6.75	6.45	5.13
8	$\Delta m^2_{21}\left(10^{-5}\ \mathrm{eV}^2\right)$	15.15	10.05	7.05	6.89	5.44
10		15.38	10.25	7.25	7.09	5.54
12		15.73	10.53	7.37	7.12	5.74
14		15.95	10.74	7.49	7.22	5.81
2		2.32	2.41	2.46	2.47	2.51
4		2.28	2.35	2.44	2.45	2.49
6		2.25	2.29	2.42	2.44	2.47
8	$\left\|\Delta m^2_{31}\right\|\left(10^{-3}\ \mathrm{eV}^2\right)$	2.23	2.27	2.41	2.43	2.46
10		2.22	2.25	2.40	2.42	2.45
12		2.21	2.24	2.40	2.42	2.43
14		2.20	2.22	2.39	2.41	2.42
2		239.899	239.932	239.95	239.960	239.978
4		239.897	239.922	239.94	239.956	239.976
6		239.896	239.918	239.93	239.953	239.974
8	$\delta_{CP}/^0$	239.891	239.914	239.93	239.946	239.972
10		239.884	239.912	239.93	239.944	239.969
12		239.881	239.911	239.93	239.942	239.965
14		239.879	239.909	239.92	239.937	239.962

representative case, we choose $M_R = 10^{14}$ GeV for $\tan\beta = 40$ in both NH and IH models. For simplicity of comparison, the results for other choices of M_R are also presented. To study the stability criteria of neutrino mass model, we start with arbitrary high energy scale input values of neutrino masses and mixings which satisfy certain conditions including Planck cosmological bound. The input value for the Dirac CP phase angle is taken at 240^0

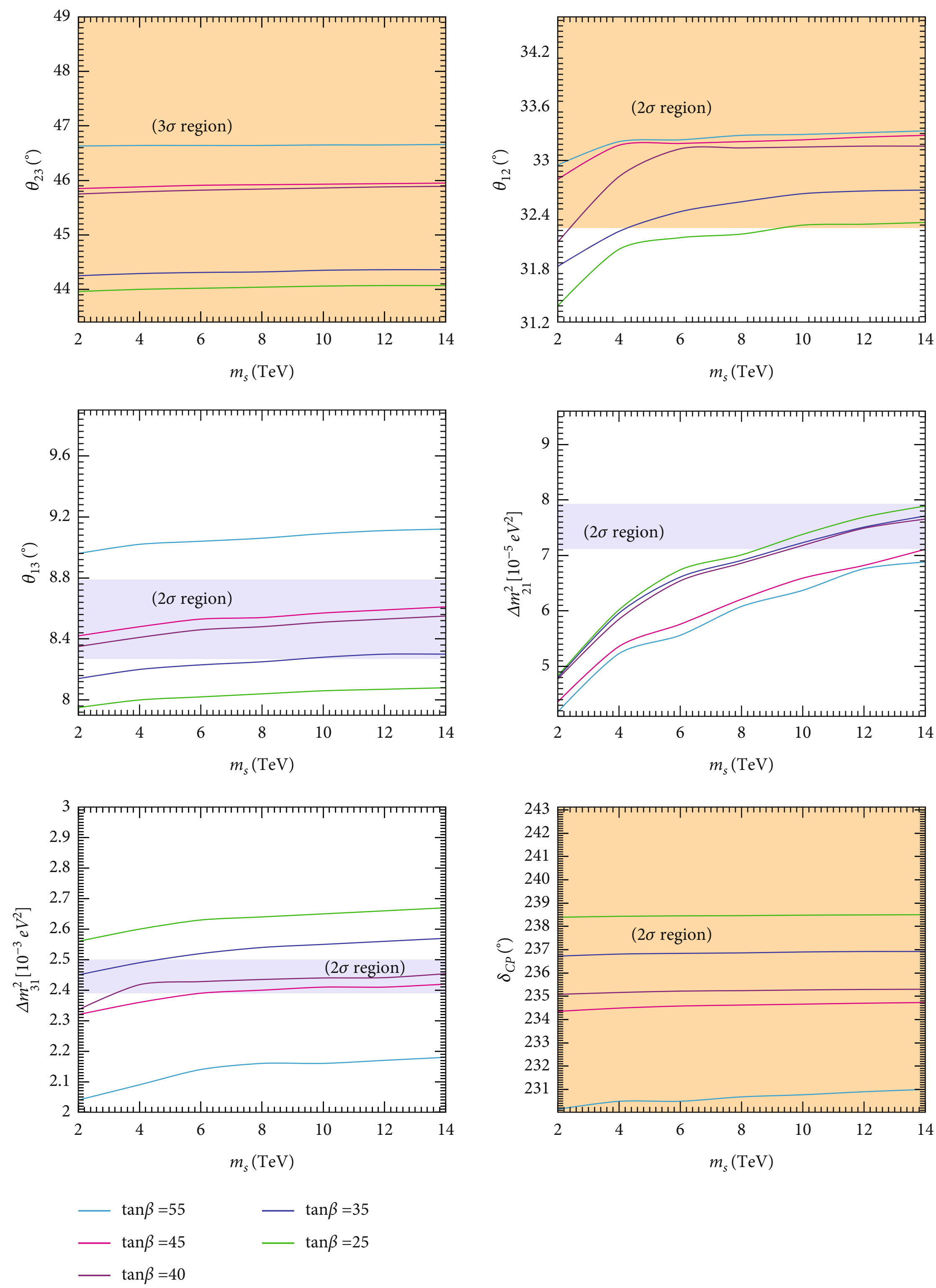

FIGURE 3: Effects on the low energy output results in θ_{ij}, $|\Delta m^2_{ij}|$, and δ_{CP} with variation of m_s for NH case at $M_R = 10^{14}$ GeV. Five different choices of $\tan\beta$ are presented.

for all cases and two Majorana phase angles at 180^0 for simplicity. In order to avoid any possible singularity in running RGEs for nearly quasidegenerate case, we considered Majorana CP conserving parity in the mass eigenvalues $(m_1,-m_2,-m_3)$. Majorana phases are more insensitive as compared to δ_{CP} against RGEs analysis and we omit to report these results. We conclude with the following important points of our results.

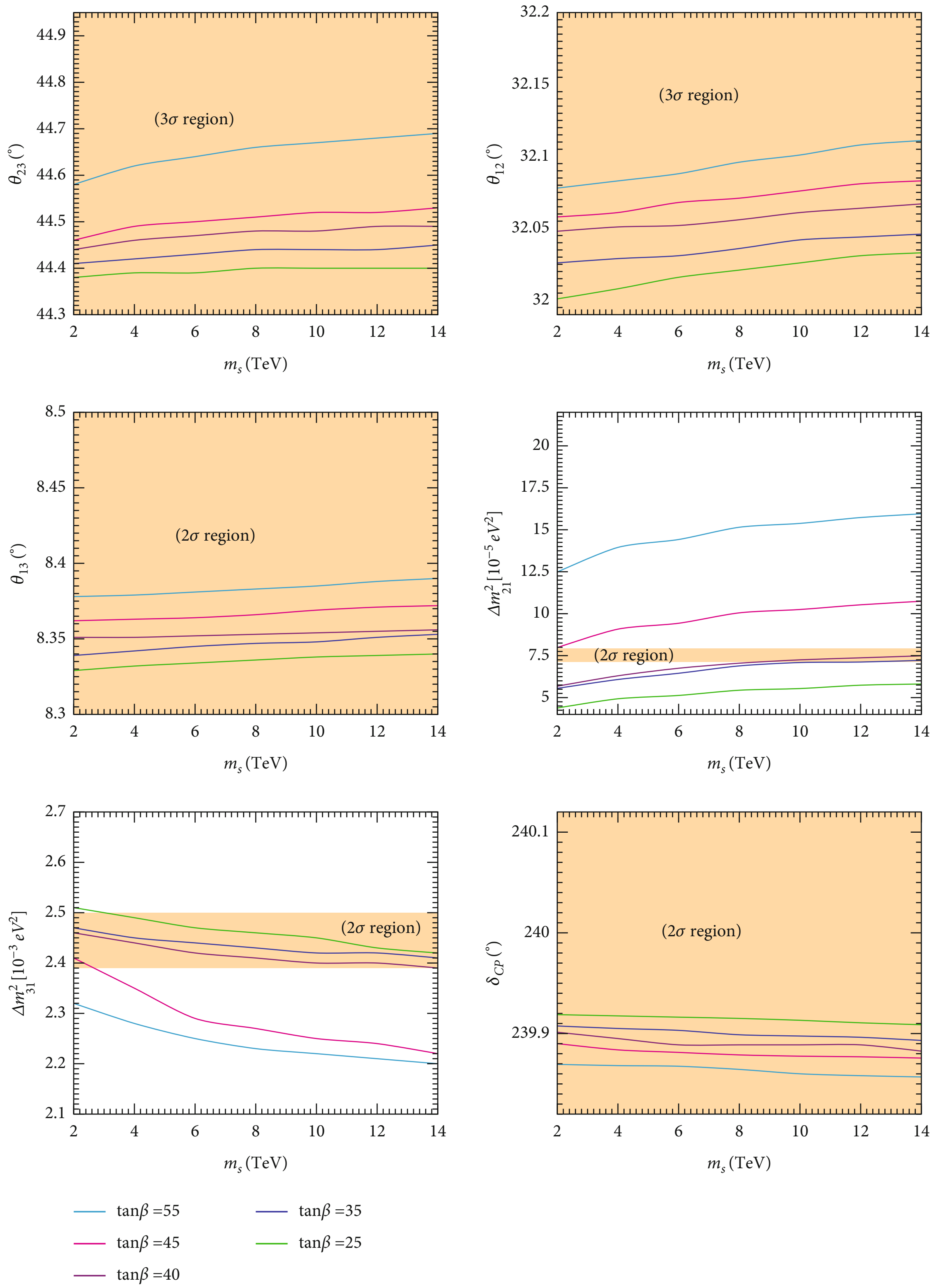

Figure 4: Effects on the low energy output results in θ_{ij}, $|\Delta m^2_{ij}|$, and δ_{CP} with variation of m_s for IH case at $M_R = 10^{14}$ GeV. Five different choices of tan β are presented.

The input value of tan β sharply affects the evolution pattern of the third generation Yukawa coupling constants (h_t, h_b, and h_τ) with energy scale. It has been observed that h_t at M_R scale always decreases with the increase of SUSY breaking scale m_s for both low and large tan β values. However, the high energy scale values of h_b and h_τ are observed to increase with the increase in m_s scale for low $\tan\beta$ values, but decrease with m_s for larger $\tan\beta$ values. For moderate $\tan\beta$ values, h_b decreases with m_s again but h_τ increases with m_s.

(i) The effect of the variation of m_s scale on neutrino oscillation parameters at low energy scale is very mild except Δm^2_{21} which is very sensitive with m_s and $\tan\beta$ values. Both low energy scale values of $|\Delta m^2_{31}|$ and Δm^2_{21} increase with the increase in m_s scale for NH case. However, Δm^2_{21} increases with the increase of m_s, but $|\Delta m^2_{31}|$ decreases with m_s for IH case. The low energy scale values of three mixing angles (θ_{12}, θ_{13}, and θ_{23}) have mild increasing trend with the increase of m_s scale for both NH and IH cases. The Dirac CP phase δ_{CP} at low energy scale increases with the increase in m_s for NH but it decreases with m_s for IH case

The simultaneous variations of m_s and $\tan\beta$ on low scale neutrino oscillation parameters have significant effects. It is observed that all the low energy values of mixing angles (θ_{12}, θ_{13}, and θ_{23}) increase with the increase in m_s and $\tan\beta$ values for both NH and IH. Both low energy values of Δm^2_{21} and $|\Delta m^2_{31}|$ decrease with the increase of $\tan\beta$, but they increase with m_s scale for NH. For IH case, Δm^2_{21} increases and $|\Delta m^2_{31}|$ decreases with the increase of m_s and $\tan\beta$. The Dirac CP phase δ_{CP} decreases with the increase of $\tan\beta$ but increases with the increase of m_s for NH case. For IH case, the low energy value of δ_{CP} decreases with the increase of both $\tan\beta$ and m_s.

The complementarity relation (SC) is found to satisfy at high and low energy scale under RGEs with the variations of both $\tan\beta$ and m_s scale.

The numerical analysis in the present work shows the stability of both NH and IH neutrino mass models with the variation of SUSY breaking scale m_s, and also the other two input parameters M_R scale $\tan\beta$ for a wide range of input values. The present analysis can be applied to check the validity at low energy scale of certain mixing patterns such as tribimaximal [51–54] and golden ratio mixing patterns defined at high energy scale [34, 55–58].

Appendix

A. RGEs for Gauge Couplings [39]

The two-loop RGEs for gauge couplings are given by

$$\frac{dg_i}{dt} = \frac{b_i}{16\pi^2} g_i^3 + \frac{1}{(16\pi^2)^2}\left[\sum_{j=1}^{3} b_{ij} g_i^3 g_j^2 - \sum_{j=t,b,\tau} a_{ij} g_i^3 h_j^2\right], \tag{A.1}$$

where $t = \ln\mu$, and b_i, b_{ij}, a_{ij} are β function coefficients in MSSM,

$$b_i = (6.6, 1.0, -3.0),\; b_{ij} = \begin{pmatrix} 7.96 & 5.40 & 17.60 \\ 1.80 & 25.00 & 24.00 \\ 2.20 & 9.00 & 14.00 \end{pmatrix},$$
$$a_{ij} = \begin{pmatrix} 5.2 & 2.8 & 3.6 \\ 6.0 & 6.0 & 2.0 \\ 4.0 & 4.0 & 0.0 \end{pmatrix}, \tag{A.2}$$

and, for non-supersymmetric case, we have

$$b_i = (4.100, -3.167, -7.00),\; b_{ij} = \begin{pmatrix} 3.98 & 2.70 & 8.8 \\ 0.90 & 5.83 & 12.0 \\ 1.10 & 4.50 & -26.0 \end{pmatrix},$$
$$a_{ij} = \begin{pmatrix} 0.85 & 0.5 & 0.5 \\ 1.50 & 1.5 & 0.5 \\ 2.00 & 2.0 & 0.0 \end{pmatrix}. \tag{A.3}$$

A.1. Two-Loop RGEs for Yukawa Couplings and Quartic Higgs Coupling [39]. For MSSM,

$$\begin{aligned}\frac{dh_t}{dt} &= \frac{h_t}{16\pi^2}\left(6h_t^2 + h_b^2 - \sum_{i=1}^{3} c_i g_i^2\right) \\ &+ \frac{h_t}{(16\pi^2)^2}\left[\sum_{i=1}\left(c_i b_i + \frac{c_i^2}{2}\right) g_i^4 + g_1^2 g_2^2 .\right. \\ &+ \frac{136}{45} g_1^2 g_3^2 + 8 g_2^2 g_3^2 + \left(\frac{6}{5} g_1^2 + 6 g_2^2 + 16 g_3^2\right) h_t^2 \\ &\left. + \frac{2}{5} g_1^2 h_b^2 - 22 h_t^4 . - 5 h_b^4 - 5 h_t^2 h_b^2 - h_b^2 h_\tau^2\right],\end{aligned}$$

$$\begin{aligned}\frac{dh_b}{dt} &= \frac{h_b}{16\pi^2}\left(6h_b^2 + h_\tau^2 + h_t^2 - \sum_{i=1}^{3} c_i' g_i^2\right) \\ &+ \frac{h_b}{(16\pi^2)^2}\left[\sum_{i=1}\left(c_i' b_i + \frac{ci'2}{2}\right) g_i^4 . + g_1^2 g_2^2 + \frac{8}{9} g_1^2 g_3^2\right. \\ &+ 8 g_2^2 g_3^2 + \left(\frac{2}{5} g_1^2 + 6 g_2^2 + 16 g_3^2\right) h_b^2 + \frac{4}{5} g_1^2 h_t^2 \\ &\left. + \frac{6}{5} g_1^2 h_\tau^2 . - 22 h_b^4 - 3 h_\tau^4 - 5 h_t^4 - 5 h_b^2 h_t^2 - 3 h_b^2 h_\tau^2\right],\end{aligned}$$

$$\frac{dh_\tau}{dt} = \frac{h_\tau}{16\pi^2}\left(4h_\tau^2 + 3h_b^2 - \sum_{i=1}^{3} c_i'' g_i^2\right) + \frac{h_\tau}{(16\pi^2)^2}\left[\sum_{i=1}\left(c_i'' b_i + \frac{ci''2}{2}\right) g_i^4 .. + \frac{9}{5} g_1^2 g_2^2 + \left(\frac{6}{5} g_1^2 + 6g_2^2\right) h_\tau^2 + \left(\frac{-2}{5} g_1^2 + 16 g_3^2\right) h_b^2 + 9g_b^4 .. - 10h_\tau^4 - 3h_b^2 h_t^2 - 9h_b^2 h_\tau^2\right], \tag{A.4}$$

where

$$c_i = \left(\frac{13}{15}, 3, \frac{16}{13}\right), c_i' = \left(\frac{7}{15}, 3, \frac{16}{3}\right), \quad c_i'' = \left(\frac{9}{5}, 3, 0\right). \tag{A.5}$$

For non-supersymmetric case,

$$\frac{dh_t}{dt} = \frac{h_t}{16\pi^2}\left(\frac{3}{2}h_t^2 - \frac{3}{2}h_b^2 + Y_2(S) - \sum_{i=1}^{3} c_i g_i^2\right) + \frac{h_t}{(16\pi^2)^2}\left[\left(\frac{1187}{600}\right) g_1^4 - \frac{23}{4} g_2^4 .. - 108 g_3^4 - \frac{9}{20} g_1^2 g_2^2 + \frac{19}{15} g_1^2 g_3^2 + 9 g_3^2 g_2^2 + \left(\frac{223}{80} g_1^2 + \frac{135}{16} g_2^2 + 16 g_3^2\right) h_t^2 . - \left(\frac{43}{80} g_1^2 - \frac{9}{16} g_2^2 + 16 g_3^2\right) h_b^2 + \frac{5}{2} Y_4(S) - 2\lambda\left(3h_t^2 + h_b^2\right) + \frac{3}{2} h_t^4 - \frac{5}{4} h_t^2 h_b^2 . + \frac{11}{4} h_b^4 + Y_2(S)\left(\frac{5}{4} h_b^2 - \frac{9}{4} h_t^2\right) - \eta_4(S) + \frac{3}{2}\lambda^2\right],$$

$$\frac{dh_b}{dt} = \frac{h_b}{16\pi^2}\left(\frac{3}{2}h_b^2 - \frac{3}{2}h_t^2 + Y_2(S) - \sum_{i=1}^{3} c_i' g_i^2\right) + \frac{h_b}{(16\pi^2)^2}\left[-\frac{127}{600} g_1^4 - \frac{23}{4} g_2^4 - 108 g_3^4 .. - \frac{27}{20} g_1^2 g_2^2 + \frac{31}{15} g_1^2 g_3^2 + 9 g_3^2 g_2^2 - \left(\frac{79}{80} g_1^2 - \frac{9}{16} g_2^2 + 16 g_3^2\right) h_t^2 + \left(\frac{187}{80} g_1^2 + \frac{135}{16} g_2^2 . + 16 g_3^2\right) h_b^2 + \frac{5}{2} Y_4(S) - 2\lambda\left(3h_t^2 + 3h_b^2\right) + \frac{3}{2} h_b^4 - \frac{5}{4} h_t^2 h_b^2 + \frac{11}{4} h_t^4 .. + Y_2(S)\left(\frac{5}{4} h_t^2 - \frac{9}{4} h_b^2\right) - \eta_4(S) + \frac{3}{2}\lambda^2\right],$$

$$\frac{dh_\tau}{dt} = \frac{h_\tau}{16\pi^2}\left(\frac{3}{2}h_\tau^2 + Y_2(S) - \sum_{i=1}^{3} c_i'' g_i^2\right) + \frac{h_\tau}{(16\pi^2)^2}\left[\frac{1371}{200} g_1^4 - \frac{23}{4} g_2^4 - \frac{27}{20} g_1^2 g_2^2 .. + \left(\frac{387}{80} g_1^2 + \frac{135}{16} g_2^2\right) h_\tau^2 + \frac{5}{2} Y_4(S) - 6\lambda h_t^2 + \frac{3}{2} h_\tau^4 - \frac{9}{4} Y_2(S) h_\tau^2 .. - \eta_4(S) + \frac{3}{2}\lambda^2\right],$$

$$\frac{d\lambda}{dt} = \frac{1}{16\pi^2}\left[\frac{9}{4}\left(\frac{3}{25} g_1^4 + \frac{2}{5} g_2^2 g_1^2 + g_2^4\right) - \left(\frac{9}{5} g_1^2 + 9 g_2^2\right)\lambda + 4Y_2(S)\lambda - 4H(S) + 12\lambda^2\right] .. + \frac{1}{(16\pi^2)^2}\left[-78\lambda^3 + 18\left(\frac{3}{5} g_1^2 + 3 g_2^2\right)\lambda^2 + \left(-\frac{73}{8} g_2^4 + \frac{117}{20} g_1^2 g_2^2 + \frac{1887}{200} g_1^4\right)\lambda .. + \frac{305}{8} g_2^6 - \frac{867}{120} g_1^2 g_2^4 - \frac{1677}{200} g_1^4 g_2^2 - \frac{3411}{1000} g_1^6 - 64 g_3^2\left(h_t^4 + h_b^4\right) - \frac{8}{5} g_1^2\left(2h_t^4 - h_b^4 .. + 3h_\tau^4\right) - \frac{3}{2} g_2^4 Y_2(S) + 10\lambda Y_4(S) + \frac{3}{5} g_1^2\left(-\frac{57}{10} g_1^2 + 21 g_2^2\right) h_t^2 + \left(\frac{3}{2} g_1^2 + 9 g_2^2\right) h_b^2 .. + \left(-\frac{15}{2} g_1^2 + 11 g_2^2\right) h_\tau^2 - 24\lambda^2 Y_2(S) - \lambda H(S) + 6\lambda h_t^2 h_b^2 + 20\left(3h_t^6 + 3h_b^6 + h_\tau^6\right) .. - 12\left(h_t^4 h_b^2 + h_t^2 h_b^4\right)\right], \tag{A.6}$$

where

$$Y_2(S) = 3h_t^2 + 3h_b^2 + h_\tau^2, \quad Y_4(S) = \frac{1}{3}\left[3\Sigma c_i g_i^2 h_t^2 + 3\Sigma c_i' g_i^2 h_b^2 + 3\Sigma c_i'' g_i^2 h_\tau^2\right], \quad H(S) = 3h_t^4 + 3h_b^4 + h_\tau^4, \quad \eta_4(S) = \frac{9}{4}\left[3h_t^4 + 3h_b^4 + h_\tau^4 - \frac{2}{3} h_t^2 h_b^2\right], \tag{A.7}$$

and $\lambda = m_h^2/v_0^2$ is the Higgs self-coupling, $m_h = 125.78 \pm 0.26\,\text{GeV}$ is the Higgs mass [59], and $v_0 = 174\,\text{GeV}$ is the vacuum expectation value.

The beta function coefficients for non-SUSY case are given below

$c_i = (0.85, 2.25, 8.00)$, $c_i' = (0.25\ 2.25, 8.00)$, and $c_i'' = (2.25\ , 2.25, 0.00)$.

B. RGEs for Three Neutrino Mixing Angles and Phases [33]: (Neglecting Higher Order of θ_{13})

$$\begin{aligned}
\dot{\theta}_{12} &= -\frac{Cy_\tau^2}{32\pi^2}\sin 2\theta_{12}s_{23}^2\frac{\left|m_1e^{i\psi_1}+m_2e^{i\psi_2}\right|^2}{\Delta m_{21}^2},\\
\dot{\theta}_{13} &= \frac{Cy_\tau^2}{32\pi^2}\sin 2\theta_{12}\sin 2\theta_{23}\frac{m_3}{\Delta m_{31}^2(1+\xi)}\\
&\quad\times[m_1\cos(\psi_1-\delta)-(1+\xi)m_2\cos(\psi_2-\delta)\\
&\quad-\xi m_3\cos\delta],\\
\dot{\theta}_{23} &= -\frac{Cy_\tau^2}{32\pi^2}\sin 2\theta_{23}\frac{1}{\Delta m_{31}^2}\left[c_{12}^2\left|m_2e^{i\psi_2}+m_3\right|^2\right.\\
&\quad\left.+s_{12}^2\frac{\left|m_1e^{i\psi_1}+m_3\right|^2}{1+\xi}\right],
\end{aligned}\tag{B.1}$$

where $\Delta m_{21}^2=m_2^2-m_1^2$, $\Delta m_{31}^2=m_3^2-m_1^2$, and $\xi=\Delta m_{21}^2/\Delta m_{31}^2$.

B.1 RGEs for the Three Phases [33]. For Dirac phase δ,

$$\dot{\delta}=\frac{Cy_\tau^2}{32\pi^2}\frac{\delta^{(-1)}}{\theta_{13}}+\frac{Cy_\tau^2}{8\pi^2}\delta^{(0)},\tag{B.2}$$

where

$$\begin{aligned}
\delta^{(-1)} &= \sin 2\theta_{12}\sin 2\theta_{23}\frac{m_3}{\Delta m_{31}^2(1+\xi)}\\
&\quad\times[m_1\sin(\psi_1-\delta)..-(1+\xi)m_2\sin(\psi_2-\delta)\\
&\quad+\xi m_3\sin\delta],
\end{aligned}\tag{B.3}$$

$$\begin{aligned}
\delta^{(0)} &= \frac{m_1m_2s_{23}^2\sin(\psi_1-\psi_2)}{\Delta m_{21}^2}..\\
&\quad+m_3s_{12}^2\left[\frac{m_1\cos 2\theta_{23}\sin\psi_1}{\Delta m_{31}^2(1+\xi)}+\frac{m_2c_{23}^2\sin(2\delta-\psi_2)}{\Delta m_{31}^2}\right]..\\
&\quad+m_3c_{12}^2\left[\frac{m_1c_{23}^2\sin(2\delta-\psi_1)}{\Delta m_{31}^2(1+\xi)}+\frac{m_2\cos(2\theta_{23})\sin\psi_2}{\Delta m_{31}^2}\right].
\end{aligned}\tag{B.4}$$

For Majorana phase ψ_1 [33],

$$\begin{aligned}
\dot{\psi}_1 &= \frac{Cy_\tau^2}{8\pi^2}\left[m_3\cos 2\theta_{23}\frac{m_1s_{12}^2\sin\psi_1+(1+\xi)m_2c_{12}^2\sin\psi_2}{\Delta m_{31}^2(1+\xi)}\right]..\\
&\quad+\frac{Cy_\tau^2}{8\pi^2}\left[\frac{m_1m_2c_{12}^2s_{23}^2\sin(\psi_1-\psi_2)}{\Delta m_{21}^2}\right].
\end{aligned}\tag{B.5}$$

For Majorana phase ψ_2,

$$\begin{aligned}
\dot{\psi}_2 &= \frac{Cy_\tau^2}{8\pi^2}\left[m_3\cos 2\theta_{23}\frac{m_1s_{12}^2\sin\psi_1+(1+\xi)m_2c_{12}^2\sin\psi_2}{\Delta m_{31}^2(1+\xi)}\right]..\\
&\quad+\frac{Cy_\tau^2}{8\pi^2}\left[\frac{m_1m_2s_{12}^2s_{23}^2\sin(\psi_1-\psi_2)}{\Delta m_{21}^2}\right].
\end{aligned}\tag{B.6}$$

B.2 RGEs for Neutrino Mass Eigenvalues [33].

$$\begin{aligned}
\dot{m}_1 &= \frac{1}{16\pi^2}\left[\alpha+Cy_\tau^2\left(2s_{12}^2s_{23}^2+F_1\right)\right]m_1,\\
\dot{m}_2 &= \frac{1}{16\pi^2}\left[\alpha+Cy_\tau^2\left(2c_{12}^2s_{23}^2+F_2\right)\right]m_2,\\
\dot{m}_3 &= \frac{1}{16\pi^2}\left[\alpha+2Cy_\tau^2c_{13}^2c_{23}\right]m_3,
\end{aligned}\tag{B.7}$$

where

$$\begin{aligned}
F_1 &= -s_{13}\sin 2\theta_{12}\sin 2\theta_{23}\cos\delta+2s_{13}^2c_{12}^2c_{23}^2,\\
F_2 &= s_{13}\sin 2\theta_{12}\sin 2\theta_{23}\cos\delta+2s_{13}^2s_{12}^2s_{23}^2.
\end{aligned}\tag{B.8}$$

For MSSM case,

$$\begin{gathered}
\alpha=-\frac{6}{5}g_1^2-6g_2^2+6y_t^2,\\
C=1.
\end{gathered}\tag{B.9}$$

For SM case,

$$\begin{gathered}
\alpha=-3g_2^2+2y_\tau^2+6y_t^2+6y_b^2+\lambda,\\
C=-\frac{3}{2},
\end{gathered}\tag{B.10}$$

and λ is the Higgs self-coupling in the SM.

Data Availability

Data related to this work can be accessed through my zenodo doi:10.5281/zenodo.6585877

Disclosure

This article is submitted to arXiv:2205.10005. This paper has been returned to draft for the presentation of the manuscript in Research Gate:https://www.researchgate.net/publication/360781986_Effects_of_variations_of_SUSY_breaking_scale_on_neutrino_parameters_at_low_energy_scale_under_radiative_corrections.

Conflicts of Interest

The authors declare that there is no conflict of interest regarding the publication of this paper.

Acknowledgments

This article is funded by the Sponsoring Consortium for Open Access Publishing in Particle Physics. One of the authors (KHD) would like to thank the Sponsoring Consortium for Open Access Publishing in Particle Physics for the support.

References

[1] D. Adey, F. P. An, A. B. Balantekin et al., "Measurement of the electron antineutrino oscillation with 1958 days of operation at Daya bay," *Physical Review Letters*, vol. 121, no. 24, article 241805, 2018.

[2] Y. Abe, C. Aberle, T. Akiri et al., "Indication of reactor $\bar{\nu}_e$ disappearance in the Double Chooz experiment," *Physical Review Letters*, vol. 108, article 131801, 2012.

[3] G. Bak, J. H. Choi, H. I. Jang et al., "Measurement of reactor antineutrino oscillation amplitude and frequency at RENO," *Physical Review Letters*, vol. 121, no. 20, article 201801, 2018.

[4] J. L. Miller, "Accelerator experiments are closing in on neutrinoCPviolation," *Physics Today*, vol. 73, no. 6, pp. 14–16, 2020.

[5] The T2K Collaboration, "Constraint on the matter–antimatter symmetry-violating phase in neutrino oscillations," *Nature*, vol. 580, no. 7803, pp. 339–344, 2020.

[6] Y. Fukuda, T. Hayakawa, E. Ichihara et al., "Evidence for oscillation of atmospheric neutrinos," *Physical Review Letters*, vol. 81, no. 8, pp. 1562–1567, 1998.

[7] Q. R. Ahmad, R. C. Allen, T. C. Andersen et al., "Direct evidence for neutrino flavor transformation from neutral current interactions in the Sudbury neutrino observatory," *Physical Review Letters*, vol. 89, no. 1, article 011301, 2002.

[8] M. C. Gonzalez-Garcia, M. Maltoni, and T. Schwetz, "NuFIT: three-flavour global analyses of neutrino oscillation experiments," *Universe*, vol. 7, no. 12, p. 459, 2021.

[9] S. Alam, M. Aubert, S. Avila et al., "Completed sdss-iv extended baryon oscillation spectroscopic survey: cosmological implications from two decades of spectroscopic surveys at the apache point observatory," *Physical Review D*, vol. 103, article 083533, 2021.

[10] N. Aghanim, Y. Akrami, M. Ashdown et al., "Planck 2018 results-VI. Cosmological parameters," *Astronomy & Astrophysics*, vol. 1, no. 641, p. A6, 2020.

[11] D. Q. Adams, C. Alduino, K. Alfonso et al., "Improved limit on neutrinoless double-beta decay in ^{130}Te with CUORE," *Physical review letters*, vol. 124, no. 12, article 122501, 2020.

[12] M. Agostini, G. R. Araujo, A. M. Bakalyarov et al., "Final results of GERDA on the search for neutrinoless double-β decay," *Physical Review Letters*, vol. 125, no. 25, article 252502, 2020.

[13] S. Abe and Zen Collaboration, "First search for the majorana nature of neutrinos in the inverted mass ordering region with KamLAND-Zen," 2022, https://arxiv.org/abs/2203.02139.

[14] M. Aker, A. Beglarian, J. Behrens et al., "Direct neutrino-mass measurement with sub-electronvolt sensitivity," *Nature Physics*, vol. 18, no. 2, pp. 160–166, 2022.

[15] S. Dimopoulos, S. Raby, and F. Wilczek, "Supersymmetry and the scale of unification," *Physical Review D*, vol. 24, no. 6, pp. 1681–1683, 1981.

[16] N. Haba and T. Ota, "Vanishing dimension five proton decay operators in the SU(5) SUSY GUT," *Acta Physica Polonica B*, vol. 39, pp. 1901–1912, 2008.

[17] S. Heinemeyer, M. Mondragón, G. Patellis, N. Tracas, and G. Zoupanos, "The Higgs boson discovery: recent implications for the finite unified theories and SUSY breaking scale," *Elementary Particle Physics and Gravity*, vol. CORFU2017, p. 81, 2018.

[18] K. S. Singh and N. N. Singh, "Effects of the variation of SUSY breaking scale on Yukawa and gauge couplings unification," *Advances in High Energy Physics*, vol. 2015, Article ID 652029, 8 pages, 2015.

[19] P. Langacker and M. Luo, "Implications of precision electroweak experiments for m_t, ρ_0, $\sin^2\theta_W$, and grand unification," *Physical Review D*, vol. 44, no. 3, p. 817, 1991.

[20] N. N. Singh and S. B. Singh, "Third generation Yukawa couplings unification in supersymmetric SO(10) model," *European Physical Journal C: Particles and Fields*, vol. 5, no. 2, pp. 363–367, 1998.

[21] S. Dawson, "Introduction to electroweak symmetry breaking," *AIP Conference Proceedings*, vol. 1116, no. 1, pp. 11–34, 2009.

[22] P. H. Chankowski and Z. Pluciennik, "Renormalization group equations for seesaw neutrino masses," *Physics Letters B*, vol. 316, no. 2-3, pp. 312–317, 1993.

[23] S. Dawson, "The MSSM and why it works," 1997, https://arxiv.org/abs/hep-ph/9712464.

[24] R. Goncalo, S. Guindon, and V. Jain, "Sensitivity of LHC experiments to the $t\bar{t}H$ final state, with $H \longrightarrow b\bar{b}$, at center of mass energy of 14 TeV," in *Contribution to Community Summer Study 2013 on the Future of U.S. Particle Physics*, p. 4, Snowmass on the Mississippi, 2013.

[25] A. K. Chaudhuri, "Large elliptic flow in low multiplicity pp collisions at LHC energy $\sqrt{s}$ = 14-TeV," *Physics Letters B*, vol. 692, pp. 15–19, 2010.

[26] E. Gibney, "How the revamped large hadron collider will hunt for new physics," *Nature*, vol. 605, no. 7911, pp. 604–607, 2022.

[27] L. Randall and M. Reece, "Single-scale natural SUSY," *Journal of High Energy Physics*, vol. 2013, article 88, 2013.

[28] K. Yonekura, "Single scale model of SUSY breaking, gauge mediation, and dark matter," *Soryushiron Kenkyu Electronics*, vol. 119, p. 1, 2011.

[29] R. L. Arnowitt and P. Nath, "Supersymmetric mass spectrum in SU(5) supergravity grand unification," *Physical Review Letters*, vol. 69, no. 5, pp. 725–728, 1992.

[30] Y. Yamada, "SUSY and GUT threshold effects in SUSY SU(5) models," *Zeitschrift für Physik*, vol. 60, pp. 83–94, 1993.

[31] D. R. T. Jones and L. Mezincescu, "The β-function in supersymmetric Yang-Mills theory," *Physics Letters B*, vol. 136, no. 4, pp. 242–244, 1984.

[32] K. S. Singh, S. Roy, and N. N. Singh, "Stability of neutrino parameters and self-complementarity relation with varying SUSY breaking scale," *Physical Review D*, vol. 97, no. 5, article 055038, 2018.

[33] S. Antusch, J. Kersten, M. Lindner, and M. Ratz, "Running neutrino masses, mixings and CP phases: analytical results and phenomenological consequences," *Nuclear Physics B*, vol. 674, no. 1-2, pp. 401–433, 2003.

[34] J. Gehrlein, S. T. Petcov, M. Spinrath, and A. V. Titov, "Renormalisation group corrections to neutrino mixing sum rules," *Journal of High Energy Physics*, vol. 2016, article 146, 2016.

[35] K. S. Babu, C. N. Leung, and J. T. Pantaleone, "Renormalization of the neutrino mass operator," *Physics Letters B*, vol. 319, no. 1-3, pp. 191–198, 1993.

[36] S. Antusch, M. Drees, J. Kersten, M. Lindner, and M. Ratz, "Neutrino mass operator renormalization revisited," *Physics Letters B*, vol. 519, no. 3-4, pp. 238–242, 2001.

[37] S. Antusch, J. Kersten, M. Lindner, M. Ratz, and M. A. Schmidt, "Running neutrino mass parameters in see-saw scenarios," *Journal of High Energy Physics*, vol. 3, p. 24, 2005.

[38] M. Chala and A. Titov, "Neutrino masses in the standard model effective field theory," *Physical Review D*, vol. 104, no. 3, article 035002, 2021.

[39] V. D. Barger, M. S. Berger, and P. Ohmann, "Supersymmetric grand unified theories: two-loop evolution of gauge and Yukawa couplings," *Physical Review D*, vol. 47, no. 3, pp. 1093–1113, 1993.

[40] Particle Data Group, "Review of particle physics," *Progress of Theoretical and Experimental Physics*, vol. 2020, no. 8, pp. 1–2093, 2020.

[41] J. E. Bjorkman and D. R. T. Jones, "The unification mass, si n$^2\theta_W$ and M_b/M_τ in nonminimal supersymmetric SU(5)," *Nuclear Physics B*, vol. 259, p. 533, 1985.

[42] M. Patgiri and N. N. Singh, "New uncertainties in QCD-QED rescaling factors using quadrature method," *Pramana*, vol. 65, pp. 1015–1025, 2006.

[43] Y. Zhang, X. Zhang, and B.-Q. Ma, "Quark-lepton complementarity and self-complementarity in different schemes," *Physical Review D*, vol. 86, article 093019, 2012.

[44] H. Minakata and A. Y. Smirnov, "Neutrino mixing and quark-lepton complementarity," *Physical Review D*, vol. 70, no. 7, article 073009, 2004.

[45] X. Zhang, "An S_4 model inspired from self-complementary neutrino mixing," *Journal of Physics G: Nuclear and Particle Physics*, vol. 45, no. 3, article 035004, 2018.

[46] M. Raidal, "Relation between the neutrino and quark mixing angles and grand unification," *Physical Review Letters*, vol. 93, no. 16, article 161801, 2004.

[47] A. Y. Smirnov, "Neutrinos: '...Annus mirabilis'," in *2nd International Workshop on Neutrino Oscillations in Venice (NO-VE 2003)*, pp. 1–21, Venice, Italy, 2004.

[48] X. Zhang and B.-Q. Ma, "On self-complementarity relations of neutrino mixing," *Physics Letters B*, vol. 710, no. 4-5, pp. 630–635, 2012.

[49] X. Zhang, Y. Zheng, and B. Q. Ma, "Quark-lepton complementarity revisited," *Physical Review D*, vol. 85, no. 9, article 097301, 2012.

[50] Y. Zheng and B. Q. Ma, "Re-evaluation of neutrino mixing pattern according to latest T2K result," *The European Physical Journal Plus*, vol. 127, no. 1, p. 7, 2012.

[51] P. F. Harrison, D. H. Perkins, and W. G. Scott, "Tri-bimaximal mixing and the neutrino oscillation data," *Physics Letters B*, vol. 530, no. 1-4, pp. 167–173, 2002.

[52] P. F. Harrison and W. G. Scott, "Symmetries and generalisations of tri-bimaximal neutrino mixing," *Physics Letters B*, vol. 535, no. 1-4, pp. 163–169, 2002.

[53] Z. Xing, "Nearly tri-bimaximal neutrino mixing and CP violation," *Physics Letters B*, vol. 533, no. 1-2, pp. 85–93, 2002.

[54] X. G. He and A. Zee, "Some simple mixing and mass matrices for neutrinos," *Physics Letters B*, vol. 560, no. 1-2, pp. 87–90, 2003.

[55] J. Zhang and S. Zhou, "Radiative corrections to the solar lepton mixing sum rule," *Journal of High Energy Physics*, vol. 2016, no. 8, article 24, pp. 1–25, 2016.

[56] J. Zhang and S. Zhou, "Viability of exact tri-bimaximal, golden-ratio and bimaximal mixing patterns and renormalization-group running effects," *Journal of High Energy Physics*, vol. 2016, article 167, 2016.

[57] Y. Kajiyama, M. Raidal, and A. Strumia, "Golden ratio prediction for solar neutrino mixing," *Physical Review D*, vol. 76, no. 11, article 117301, 2007.

[58] L. L. Everett and A. J. Stuart, "Icosahedral (A5) family symmetry and the golden ratio prediction for solar neutrino mixing," *Physical Review D*, vol. 79, no. 8, article 085005, 2009.

[59] A. Sirunyan, A. Tumasyan, W. Adam et al., "A measurement of the Higgs boson mass in the diphoton decay channel," *Physics Letters B*, vol. 805, article 135425, 2020.